Monte Carlo estimation of transverse and longitudinal correlation functions in the $O(4)$ model

J. Kaupužs [a,*], R.V.N. Melnik [b], J. Rimšāns [a]

[a] *Institute of Mathematics and Computer Science, University of Latvia, 29 Raiņa Boulevard, LV-1459 Riga, Latvia*
[b] *Wilfrid Laurier University, Waterloo, Ontario, Canada, N2L 3C5*

ABSTRACT

Monte Carlo simulations of the three-dimensional $O(4)$ model in the ordered phase are performed to study the Goldstone mode effects. Our data show a distinct scaling region, where the Fourier-transformed transverse correlation function behaves as $\propto k^{-\lambda_\perp}$ with $\lambda_\perp < 2$ ($\lambda \simeq 1.95$), in disagreement with the standard theoretical prediction $\lambda_\perp = 2$.

© 2010 Elsevier B.V. All rights reserved.

1. Introduction

Many theoretical works (see, e.g., [1–5] and references therein for the theoretical approaches further referred here as the standard theory), as well as numerical Monte Carlo (MC) studies [6–10] have been devoted to the investigation of the Goldstone mode effects in *n*-component vector–spin models, which have $O(n)$ global rotational symmetry at zero external field **h**. These are the models with the Hamiltonian $\mathcal{H}$

$$\frac{\mathcal{H}}{T} = -\beta \left(\sum_{\langle ij \rangle} \mathbf{s}_i \mathbf{s}_j + \sum_i \mathbf{h}\mathbf{s}_i \right), \tag{1}$$

where T is temperature, $\mathbf{s}_i \equiv \mathbf{s}(\mathbf{x}_i)$ is the *n*-component vector of unit length, i.e., the spin variable of the *i*-th lattice site with coordinate $\mathbf{x}_i$, and β is the coupling constant. The summation takes place over all nearest neighbors in the lattice.

Our recent MC studies of the three-dimensional (3D) XY (or $O(2)$) model have not fully confirmed with the standard theoretical predictions regarding the singularity of the magnetization $M(h)$ and the longitudinal susceptibility $\chi_\parallel(h)$ depending on the external field h at $h \to 0$, but they have rather pointed to some systematic deviations from the expected (within the standard theory) asymptotic behavior $M(h) - M(+0) \propto h^{1/2}$ and $\chi_\parallel(h) \propto h^{-1/2}$. In particular, our estimation in [10], including both leading and sub-leading

corrections to scaling, suggests that the exponent in the above asymptotic expressions should be modified as $M(h) - M(+0) \propto h^\rho$ and $\chi_\parallel(h) \propto h^{\rho-1}$ with $\rho = 0.555(17)$. These Goldstone mode singularities originate from the divergence of the Fourier-transformed transverse correlation function $G_\perp(\mathbf{k})$. The standard ansatz for small external sources $H = \beta h$ and wave vectors **k** reads [11]

$$G_\perp(\mathbf{k}) = \frac{M^2}{MH + \rho_s k^2}, \tag{2}$$

where ρ_s is the stiffness coefficient. It suggests that $G_\perp(\mathbf{k}) \propto k^{-\lambda_\perp}$ with the exponent $\lambda_\perp = 2$ holds for small wave vectors at $H = +0$. In fact, the form of this ansatz (2) is such as expected from the Gaussian spin wave theory. One claims that the simulation results for the three-dimensional $O(4)$ (i.e. $n = 4$) model [7] are well consistent with this theory. However, it is not surprising that the agreement in this case can be remarkably better than for the $O(2)$ (i.e. XY) model, since $\lambda_\perp \to 2$ is expected at $n \to \infty$ due to the known results for the spherical model corresponding to this limit.

The main goal of this Letter is to verify the consistency of our current MC data for the $O(4)$ model with the ansatz (2) and to estimate the exponent $\lambda_\perp$. The magnetization data for lattices up to the linear size $L = 120$ have been already considered in [7]. Our MC simulation results provide much more accurate estimations of the magnetization for lattices with $L \leqslant 350$. Besides, we have simulated also the transverse and longitudinal correlation functions and susceptibilities.

* Corresponding author.
E-mail address: kaupuzs@latnet.lv (J. Kaupužs).

2. Simulation method

We consider the $O(4)$ model on the simple cubic lattice with periodic boundary conditions. Hence, the spin $\mathbf{s} = (s_1, s_2, s_3, s_4)$ is a 4-component vector with $\mathbf{s}^2 = 1$. We can define that the field is oriented along the axis labeled with index 1. In this case, each spin has a longitudinal component $s_1 \equiv s_\parallel$ and transverse components s_2, s_3, s_4, which form the transverse spin vector $\mathbf{s}_\perp = (0, s_2, s_3, s_4)$.

The longitudinal component of the magnetization per spin is

$$m_\parallel = N^{-1} \sum_{\mathbf{x}} s_\parallel(\mathbf{x}), \tag{3}$$

where the summation takes place over all lattice sites with coordinates $\mathbf{x}$, and $N = L^3$ is the total number of sites for the lattice of linear size L. In the following, we will be interested in the mean magnetization of the spin system $M = \langle m_\parallel \rangle$. The longitudinal and transverse correlation functions in the coordinate representation, $\tilde{G}_\parallel(\mathbf{x})$ and $\tilde{G}_\perp(\mathbf{x})$, are defined by

$$\tilde{G}_\parallel(\mathbf{x}_2 - \mathbf{x}_1) = \langle s_\parallel(\mathbf{x}_1) s_\parallel(\mathbf{x}_2) \rangle - M^2, \tag{4}$$

$$\tilde{G}_\perp(\mathbf{x}_2 - \mathbf{x}_1) = \langle s_i(\mathbf{x}_1) s_i(\mathbf{x}_2) \rangle : \quad i = 2, 3, 4. \tag{5}$$

Due to the symmetry of the model, the correlation functions depend only on the coordinate difference $\mathbf{x}_2 - \mathbf{x}_1$ and (5) is the same for any transverse component $i = 2, 3, 4$. Accordingly, we can rewrite (5) for our n-component ($n = 4$) model as

$$\tilde{G}_\perp(\mathbf{x}_2 - \mathbf{x}_1) = \frac{1}{n-1} \langle \mathbf{s}_\perp(\mathbf{x}_1) \mathbf{s}_\perp(\mathbf{x}_2) \rangle. \tag{6}$$

The standard Wolff algorithm [12] is designed for Monte Carlo simulations in zero external field $h = 0$. Here we use the modified Wolff algorithm, as in [9,10]. In this method, the external field is introduced as an auxiliary spin of unit length $\mathbf{e}$ which interacts with all other spins by the coupling constant $|h|\beta$. This spin is treated on the same grounds as other ones, whereas the longitudinal component of spin $\mathbf{s}$ is its projection on the auxiliary spin $\mathbf{e}$. This modification is fully analogous to that used in [6] for the Swendsen–Wang algorithm. In fact, the rotational symmetry of model is used here, according to which an equivalent spin configuration with the same statistical weight is obtained if the external field together with all spins are rotated by any angle. Thus, in this simulation algorithm, the longitudinal and transverse spin components are given by

$$s_\parallel(\mathbf{x}) = \mathbf{s}(\mathbf{x}) \cdot \mathbf{e}, \tag{7}$$

$$\mathbf{s}_\perp(\mathbf{x}) = \mathbf{s}(\mathbf{x}) - s_\parallel(\mathbf{x})\mathbf{e}. \tag{8}$$

Eqs. (3), (4), and (6) are valid in this case, since the scalar product is invariant with respect to the rotation of coordinate system.

The Fourier-transformed longitudinal and transverse correlation functions are

$$G_\parallel(\mathbf{k}) = N^{-1} \sum_{\mathbf{x}} \tilde{G}_\parallel(\mathbf{x}) e^{-i\mathbf{k}\mathbf{x}} = \langle |\grave{s}_\parallel(\mathbf{k})|^2 \rangle - \delta_{\mathbf{k},\mathbf{0}} N M^2, \tag{9}$$

$$G_\perp(\mathbf{k}) = N^{-1} \sum_{\mathbf{x}} \tilde{G}_\perp(\mathbf{x}) e^{-i\mathbf{k}\mathbf{x}} = \frac{1}{n-1} \left\langle \sum_{i=1}^{n} |\grave{s}_{\perp,i}(\mathbf{k})|^2 \right\rangle, \tag{10}$$

where $\grave{s}_\parallel(\mathbf{k})$ is the Fourier transform of $s_\parallel(\mathbf{x})$ and $\grave{s}_{\perp,i}(\mathbf{k})$ is the Fourier transform of $s_{\perp,i}(\mathbf{x})$, the latter being the i-th component of $\mathbf{s}_\perp(\mathbf{x})$ in (8). These Fourier transforms are defined by

$$\grave{s}_\parallel(\mathbf{k}) = N^{-1/2} \sum_{\mathbf{x}} s_\parallel(\mathbf{x}) e^{-i\mathbf{k}\mathbf{x}}, \tag{11}$$

$$\grave{s}_{\perp,i}(\mathbf{k}) = N^{-1/2} \sum_{\mathbf{x}} s_{\perp,i}(\mathbf{x}) e^{-i\mathbf{k}\mathbf{x}}. \tag{12}$$

In such a way, we have to make an averaging over a set of MC measurements of $|\grave{s}_\parallel(\mathbf{k})|^2$ and $|\grave{s}_{\perp,i}(\mathbf{k})|^2$ to determine the Fourier-transformed correlation functions. We have evaluated them for the wave vectors $\mathbf{k}_\ell = (0, 0, k_\ell)$ parallel to the z axis, where $k_\ell = (2\pi/L)\ell$. Denoting the coordinate vector as $\mathbf{x} = (x, y, z)$, where $x, y, z = 0, 1, \ldots, L-1$, the scalar product $\mathbf{k}_\ell \mathbf{x} = z k_\ell$ is independent of the coordinates x and y in this case. Using (11) and (12), it yields

$$|\grave{s}_\parallel(\mathbf{k}_\ell)|^2 = N^{-1} \left[\left(\sum_{z=0}^{L-1} \hat{s}_\parallel(z) \cos(k_\ell z) \right)^2 \right.$$
$$\left. + \left(\sum_{z=0}^{L-1} \hat{s}_\parallel(z) \sin(k_\ell z) \right)^2 \right], \tag{13}$$

$$|\grave{s}_{\perp,i}(\mathbf{k}_\ell)|^2 = N^{-1} \left[\left(\sum_{z=0}^{L-1} \hat{s}_{\perp,i}(z) \cos(k_\ell z) \right)^2 \right.$$
$$\left. + \left(\sum_{z=0}^{L-1} \hat{s}_{\perp,i}(z) \sin(k_\ell z) \right)^2 \right], \tag{14}$$

where

$$\hat{s}_\parallel(z) = \sum_{x,y=0}^{L-1} s_\parallel(x, y, z), \qquad \hat{s}_{\perp,i}(z) = \sum_{x,y=0}^{L-1} s_{\perp,i}(x, y, z) \tag{15}$$

are the sums over a particular plane with given coordinate z. Using (13)–(15), the direct Monte Carlo estimation of the Fourier-transformed correlation functions (9) and (10) for the given set of wave vectors is done very efficiently, so that it even does not require any remarkable extra computation time as compared to a simulation where only the magnetization and susceptibilities are measured. As it is well known [13], the longitudinal and transverse susceptibilities, $\chi_\parallel$ and $\chi_\perp$, are related to the corresponding correlation functions at zero wave vector, i.e.,

$$\chi_\parallel = G_\parallel(\mathbf{0}) = N(\langle m_\parallel^2 \rangle - \langle m_\parallel \rangle^2), \tag{16}$$

$$\chi_\perp = G_\perp(\mathbf{0}). \tag{17}$$

It is convenient to use the Cartesian coordinates for $\mathbf{e}$ and $\mathbf{s}$ to implement all these calculations. In the Wolff algorithm, the spins of a cluster are reflected with respect to a plane, which is perpendicular to a randomly chosen unit vector $\mathbf{r} = (r_1, \ldots, r_n)$. The distribution of $\mathbf{r}$ must be spherically symmetrical. We have generated it by a method, which is valid for any number of vector components n, and consists of two steps: (i) generate n uniformly distributed within $[-1, 1]$ random numbers $r_1, r_2, \ldots, r_n$, repeating this step until $\sum_i r_i^2 \leqslant 1$ holds (it yields $\mathbf{r}$ uniformly distributed inside the unit sphere), and (ii) renormalize the final set of vector coordinates $r_i \to r_i / \sqrt{\sum_i r_i^2}$ so that $|\mathbf{r}| = 1$ holds. The reflection of a spin, $\mathbf{s} \to \mathbf{s} - 2(\mathbf{sr})\mathbf{r}$, is straightforward in the Cartesian coordinates. In this case we treat all spin components independently. In exact arithmetics, it ensures that $|\mathbf{s}| = 1$ always holds. In computer calculations some deviations occur because of an accumulation of numerical errors. In our simulations, we have corrected them by setting $s_i \to s_i / \sqrt{\sum_i s_i^2}$ after each 100 cluster algorithm steps. The observed deviations of $|\mathbf{s}|$ from unity were extremely small and never exceeded 10^{-14}. Alternatively, one could treat only $n-1$ components independently. However, it slows down the simulation remarkably, since one needs to calculate the square root $s_n = \sqrt{1 - \sum_{i=1}^{n-1} s_i^2}$ frequently.
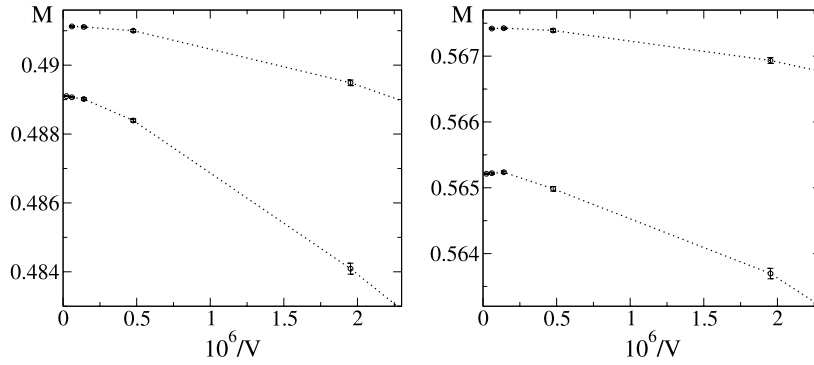
Fig. 1. Plots of the magnetization as a function of the inverse volume $1/V$ at $\beta = 1.1$ (left) and $\beta = 1.2$ (right). The external field is $h = 0.0003125$ for the lower plot and $h = 0.000625$ for the upper plot at $\beta = 1.1$. The corresponding values are $h = 0.000625$ and $h = 0.00125$ at $\beta = 1.2$. The shown here data points correspond to the sizes $L = 80, 128, 192, 256, 350$.

Table 1

The simulated values of the magnetization $\langle m_\parallel \rangle$ and the longitudinal susceptibility $\chi_\parallel$ depending on the external field h at $\beta = 1.1$. Here L and L' are the two largest sizes simulated at the given h.

$10^4 h$	L	L'	$\langle m_\parallel \rangle(L)$	$\langle m_\parallel \rangle(L')$	$\chi_\parallel(L)$	$\chi_\parallel(L')$
3.125	350	256	0.4891004(97)	0.489068(14)	7.17(13)	7.31(13)
4.375	350	256	0.4900007(84)	0.490003(12)	6.20(12)	6.06(10)
6.25	256	192	0.491124(15)	0.491110(21)	5.27(12)	5.174(98)
8.75	256	192	0.4924416(80)	0.492444(11)	4.312(51)	4.321(52)
12.5	256	192	0.494065(10)	0.494064(15)	3.752(69)	3.663(67)
17.5	256	192	0.4959221(90)	0.495927(12)	3.123(54)	3.080(45)
25	192	128	0.4982889(96)	0.498282(15)	2.574(32)	2.644(37)
35	192	128	0.5009505(93)	0.500964(12)	2.254(31)	2.230(23)
50	192	128	0.5043576(73)	0.504337(11)	1.902(25)	1.898(19)
70	192	128	0.5082070(63)	0.5081975(89)	1.626(19)	1.622(17)
100	128	64	0.5130847(69)	0.513073(16)	1.370(13)	1.3661(89)
140	128	64	0.5186193(66)	0.518616(12)	1.156(11)	1.1564(65)
200	128	64	0.5256266(57)	0.525614(12)	0.9680(91)	0.9730(62)
280	128	64	0.5334915(50)	0.5334840(92)	0.8252(68)	0.8254(47)
400	128	64	0.5433499(47)	0.5433539(81)	0.6933(61)	0.6899(37)
560	128	64	0.5543115(39)	0.5543081(85)	0.5719(41)	0.5629(32)
800	128	64	0.5678733(42)	0.5678637(74)	0.4644(36)	0.4663(25)

3. Magnetization and longitudinal susceptibility

The simulations have been performed in the ordered phase at $\beta = 1.1$ and $\beta = 1.2$, i.e., at $\beta > \beta_c$, where $\beta_c \simeq 0.93590$ [7] is the critical coupling. For each of the considered h and L values, one MC run (in few cases two runs) has been performed, which has been split into 110 bins. One bin included $\mathcal{N} = m/L$ cluster algorithm steps with $m = 768\,000$ for all L, except the largest size $L = 350$, for which $m = 770\,000$. Discarding the first 10 bins, the magnetization $\langle m_\parallel \rangle$ (3) and the longitudinal susceptibility $\chi_\parallel$ (16) have been evaluated from the remaining 100 bins, the standard error being estimated by the jackknife method [14]. For each β and h value, several sizes L have been considered. A fast convergence to certain values of $\langle m_\parallel \rangle$ and $\chi_\parallel$ for the sequence of sizes $L = 32, 64, 80, 128, 192, 256, 350$ has been observed, as it is illustrated in Fig. 1 for the magnetization as a function of $1/V$, where $V = L^3$ is the volume of the system. The decrease of the finite-size effects at $V \to \infty$ is so fast (probably, even faster than $1/V$) that the thermodynamic limit can be well estimated at appropriate largest L, chosen in such a way to ensure that the results at two largest sizes L and L' agree with each other within the statistical error bars. This L is determined for any given β and h. It increases for smaller h. Skipping smaller sizes, the simulation results for $h \leqslant 0.08$ are collected in Tables 1 and 2. An additional (second) run has been performed for $10^4 h = 3.125, 4.375, 8.75$ in order to estimate the correlation functions. The data from both runs have been used for a better evaluation of $\langle m_\parallel \rangle$ and $\chi_\parallel$ in these cases.

The simulated data at L and L' agree within the error bars of about one standard deviation σ. Hence, due to the already men-

tioned fact of the fast convergence, $\langle m_\parallel \rangle(L)$ and $\chi_\parallel(L)$ are used as the magnetization M and the susceptibility $\chi_\parallel$ of an infinite lattice in the following fits. Various ways of fitting such data have been discussed in detail in [9,10]. In the actual case of the 4-component vector model, the exponent ρ (introduced in Section 1) apparently is closer to the standard (Gaussian) theoretical value $1/2$, as compared to the XY model considered in [9,10]. Therefore we are looking for sufficiently stable methods, which would provide small enough statistical errors allowing to distinguish between $\rho = 1/2$ and $\rho \neq 1/2$ if a small deviation from the standard value really takes place, as expected from the theoretical treatment in [15–17] yielding $1/2 < \rho < 1$ and $3/2 < \lambda_\perp < 2$ in three dimensions ($d/2 < \lambda_\perp < 2$ and $\rho = (d/\lambda_\perp) - 1$ in d dimensions, where $2 < d < 4$).

The linear log–log fits of the susceptibility data over the range $h \leqslant 0.04$ are shown in Fig. 2. These give $\rho = 0.5190(22)$ at $\beta = 1.1$ and $\rho = 0.5255(27)$ at $\beta = 1.2$. The χ^2/d.o.f. (χ^2 per degree of freedom of the fit, see [14]) of these fits are 0.86 and 1.10, respectively. Thus, the fits look good and suggest that $\rho > 1/2$. However, corrections to scaling are not included here, and it is also difficult to include them keeping a high enough accuracy because of too large statistical errors in the susceptibility data.

Another possibility is to fit the magnetization data to the ansatz

$$M(h) = M(+0) + a_1 h^\rho + a_2 h, \tag{18}$$

where the first correction to scaling $a_2 h$, predicted by the standard theory, is included, keeping the leading exponent ρ as a fit parameter. It allows to test the consistency with the standard

Table 2
The simulated values of the magnetization $\langle m_\parallel \rangle$ and the longitudinal susceptibility $\chi_\parallel$ depending on the external field h at $\beta = 1.2$. Here L and L' are the two largest sizes simulated at the given h.

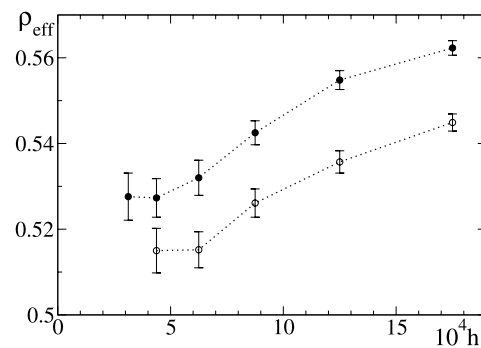| $10^4 h$	L	L'	$\langle m_\parallel \rangle (L)$	$\langle m_\parallel \rangle (L')$	$\chi_\parallel (L)$	$\chi_\parallel (L')$
4.375	350	256	0.5643787(78)	0.564385(10)	4.271(97)	4.227(76)
6.25	350	256	0.5652128(86)	0.565222(13)	3.324(91)	3.428(80)
8.75	256	192	0.5661920(73)	0.566186(11)	2.911(45)	2.950(40)
12.5	256	192	0.5674191(84)	0.567425(12)	2.447(50)	2.358(34)
17.5	256	192	0.5687855(82)	0.568802(11)	2.132(39)	2.107(37)
25	256	192	0.5705316(69)	0.5705208(82)	1.801(27)	1.750(23)
35	192	128	0.5725040(67)	0.572497(12)	1.500(22)	1.528(18)
50	192	128	0.5750064(62)	0.5749830(94)	1.276(18)	1.283(13)
70	192	128	0.5778474(55)	0.5778392(77)	1.088(14)	1.094(11)
100	192	128	0.5814603(51)	0.5814572(74)	0.919(11)	0.9147(84)
140	128	64	0.5855297(60)	0.585528(11)	0.7972(71)	0.7868(52)
200	128	64	0.5907221(55)	0.5907107(97)	0.6701(65)	0.6644(39)
280	128	64	0.5965715(42)	0.5965774(86)	0.5614(40)	0.5625(35)
400	128	64	0.6039732(38)	0.6039692(71)	0.4808(40)	0.4783(26)
560	128	64	0.6122604(36)	0.6122530(72)	0.4000(32)	0.3946(20)
800	64	32	0.6226418(64)	0.622630(12)	0.3275(21)	0.3283(12)
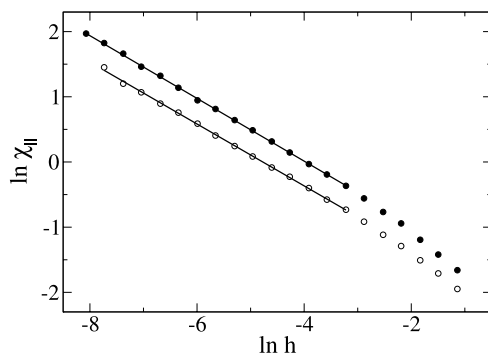
Fig. 2. The $\ln \chi_\parallel$ vs $\ln h$ plots for $\beta = 1.1$ (solid circles) and for $\beta = 1.2$ (empty circles).

Fig. 3. The effective exponent $\rho_{\text{eff}}(h)$ vs $10^4 h$ for $\beta = 1.1$ (upper plot) and $\beta = 1.2$ (lower plot).

prediction $\rho = 1/2$. In principle, higher-order corrections can also be included. However, as shown in [10] and can be verified in our case, such fits become unstable and give too large statistical errors because of too many fit parameters. So, we find that a fit to (18) with only the leading correction term included is an optimal choice. The fit over $10^4 h \in [3.125, 140]$ yields $\rho = 0.5261(37)$ (with $\chi^2/\text{d.o.f.} = 0.78$) at $\beta = 1.1$, and the fit over $10^4 h \in [4.375, 200]$ yields $\rho = 0.5161(34)$ (with $\chi^2/\text{d.o.f.} = 1.11$) at $\beta = 1.2$. The fit intervals have been chosen, discarding the largest h data points until the result is stabilized (i.e., very well agrees with that obtained by discarding one more point) and the $\chi^2/\text{d.o.f.}$ of the fit becomes acceptably small. These results, again, suggest that $\rho > 1/2$ holds. If the exponent ρ is fixed, setting $\rho = 1/2$, then the fits over these h intervals are not satisfactory, i.e., $\chi^2/\text{d.o.f.} = 6.17$ at $\beta = 1.1$ and $\chi^2/\text{d.o.f.} = 3.56$ at $\beta = 1.2$. As expected, such fits become acceptably good when the fit interval is chosen remarkably (twice) narrower, since it is always easy to fit the data over a sufficiently narrow interval.

Formally, the slight disagreement between the ρ values obtained at $\beta = 1.1$ and $\beta = 1.2$ might imply that either this exponent is not universal, or the systematic errors due to the neglected sub-leading corrections to scaling are comparable with the discrepancy about 0.01. However, according to both the standard theory and [16], the non-universality scenario should be excluded.

To analyze possible systematic errors and tendencies, we consider the effective exponent $\rho_{\text{eff}}(h)$, provided by the fit to (18) within the interval $[h, Ah]$. The coefficient $A = 32$ is chosen large enough to ensure stable results and small enough to enable acceptably good fits for several h values. We have plotted this effective exponent as a function of h in Fig. 3, since a linear behavior at

$h \to 0$ is then expected (according to the standard theory) due to the neglected sub-leading correction to scaling $\sim h^{3/2}$ in (18). According to Fig. 3, the common value to which both plots could converge, very likely, is $\rho \approx 0.52$ within the error bars about ± 0.01. Here 0.52 is the rounded to two decimal digits mean value over the fit results for $\beta = 1.1$ and $\beta = 1.2$ discussed before. The error bars include both the statistical and systematical uncertainties in this case. Since it is quite difficult to estimate possible systematic errors due to the variations of the effective exponents, we should set even larger than ± 0.01 error bars for a high enough confidence level. Thus, we have estimated $\rho = 0.52 \pm 0.02$. According to this estimation, the exponent ρ might be consistent with $1/2$ as a marginal possible value, although the most probable value is closer to 0.52, which is also proposed by the fits of the susceptibility data.

Apart from the exponent ρ, the considered fits to (18) provide the MC estimates of the spontaneous magnetization: $M(+0) = 0.484475(48)$ at $\beta = 1.1$ and $M(+0) = 0.560178(40)$ at $\beta = 1.2$. Fixing the exponent $\rho = 1/2$ in (18), we obtain $M(+0) = 0.484230(20)$ from $10^4 h \in [3.125, 50]$ at $\beta = 1.1$ and $M(+0) = 0.560028(12)$ from $10^4 h \in [4.375, 100]$ at $\beta = 1.2$. For comparison, we have made similar fits as in [7], i.e., for larger fields, neglecting corrections to scaling and setting $\rho = 1/2$. In this way we obtain $M(+0) = 0.483415(33)$ at $\beta = 1.1$ from $10^4 h \in [35, 70]$ and $M(+0) = 0.559298(24)$ at $\beta = 1.2$ from $10^4 h \in [70, 140]$ in approximate agreement with the corresponding values 0.48257(29) and 0.55911(13), reported in [7]. Our estimates provided at the beginning of this paragraph are more accurate, since they are obtained at smaller external fields, including also the leading correction to scaling.

Table 3
The test of consistency of the simulated data with (19).

β	$10^4 h$	L	$M(h)/(\beta h)$	$G_\perp(\mathbf{0})$
1.1	3.125	350	1422.837(28)	1449(75)
1.1	3.125	256	1422.744(40)	1435(63)
1.1	4.375	350	1018.183(17)	977(40)
1.1	4.375	256	1018.187(24)	1044(42)
1.1	8.75	256	511.6276(83)	481(17)
1.1	8.75	192	511.630(12)	507(16)
1.2	4.375	350	1075.007(15)	1034(57)
1.2	4.375	256	1075.020(19)	990(40)
1.2	8.75	256	539.2305(70)	532(20)
1.2	8.75	192	539.225(10)	557(22)

4. Correlation functions

The transverse and longitudinal correlation functions have been simulated at $10^4 h = 3.125$, 4.375, 8.75. In fact, the transverse susceptibility also has been simulated, since $\chi_\perp \equiv G_\perp(\mathbf{0})$ holds. As an important test of validity, we have checked how well our finite-size data for $G_\perp(\mathbf{k})$ are consistent with the known exact relation [13]

$$G_\perp(\mathbf{0}) = \frac{M(h)}{\beta h}: \quad h \to 0 \qquad (19)$$

in the thermodynamic limit. The comparison in Table 3 shows that our finite-size data for the largest lattices and the smallest fields $10^4 h = 3.125$, 4.375 are well consistent with $G_\perp(\mathbf{0})$ of an infinite lattice. Moreover, the finite-size effects decrease with k, and we observe that the plots of $\ln G_\perp(\mathbf{k})$ vs $\ln k$ for different sizes considered in Table 3, and even for remarkably smaller sizes, lie on top of each other within the statistical error bars. It is illustrated in Fig. 4, where such plots are shown at the smallest h value 0.0003125 for $\beta = 1.1$. The plots at $L = 350$, 256 and 128 perfectly lie on top of each other, and even the $L = 64$ plot is almost perfectly consistent with those of larger sizes. In the latter case only the first (smallest k) point at $L = 64$ is less well consistent with the corresponding point at $L = 256$, where the discrepancy is about two standard deviations ($\sim 2\sigma$) instead of the more usual $\sim \sigma$. Hence, even in this case we still cannot conclude that there are well detectable systematic deviations. These appear only at the smallest sizes considered, i.e., $L = 32$ (solid circles) and $L = 16$ (asterisk). Only the case $\beta = 1.1$ is shown in Fig. 4, but the finite-size behavior at $\beta = 1.2$ is quite similar, i.e., no detectable systematic deviations are observed for $64 \leqslant L \leqslant 350$. Thus, we can conclude with a great confidence that the thermodynamic limit for $G_\perp(\mathbf{k})$ at nonzero $\mathbf{k}$ is reached with a high enough accuracy (for $\mathbf{k} = 0$, it is also reached, according to the tests of consistency with (19)), and our data are well suited for the following analysis aimed to test the theoretical predictions for the transverse correlation function in the thermodynamic limit.

To show the general behavior of the correlation functions, we have plotted them in Fig. 5 for a subset of parameters. We have analyzed in detail the $G_\perp(\mathbf{k})$ data at the largest lattice size $L = 350$ to verify the standard ansatz (2), which can be written as

$$G_\perp(\mathbf{k}, h) = \frac{1}{\frac{\beta h}{M(h)} + a(h)k^2} \qquad (20)$$

for any given β. The parameter $a(h)$ has been estimated by fitting the data to (20) within $k \leqslant k_6$, where $k_l = 2\pi l/L$, yielding $a(0.0003125) = 1.222(14)$, $a(0.0004375) = 1.236(14)$ at $\beta = 1.1$ and $a(0.0004375) = 1.320(15)$ at $\beta = 1.2$.

At $h = +0$, the behavior of the transverse correlation function is power-like, i.e. $G_\perp(\mathbf{k}) \propto k^{-\lambda_\perp}$ or

$$\ln\left(k^2 G_\perp(\mathbf{k})\right) = const + (2 - \lambda_\perp) \ln k \qquad (21)$$
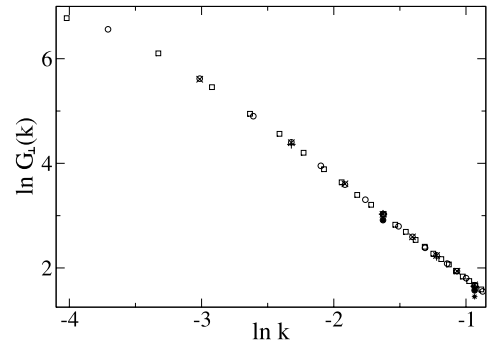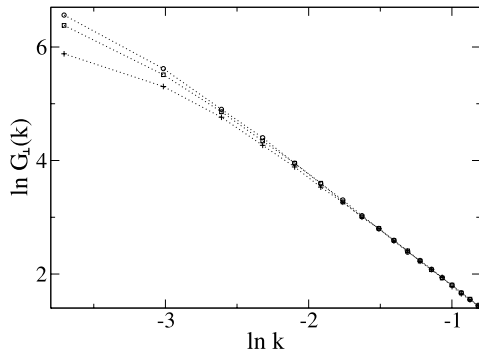

Fig. 4. Logarithm of the transverse correlation function vs $\ln k$ at $\beta = 1.1$, $h = 0.0003125$ for several system sizes: $L = 350$ (squares), $L = 256$ (empty circles), $L = 128$ (x), $L = 64$ (pluses), $L = 32$ (solid circles) and $L = 16$ (asterisk).
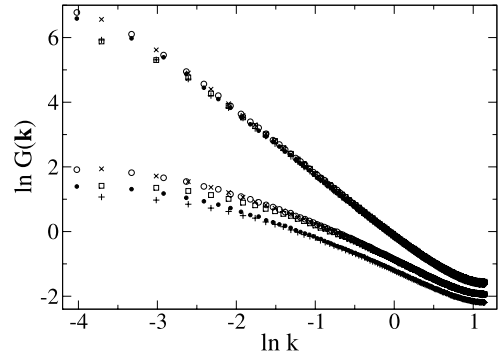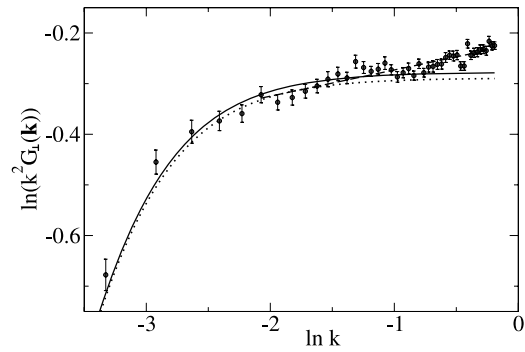

Fig. 5. Logarithm of the transverse and the longitudinal correlation function ($G(\mathbf{k}) = G_\perp(\mathbf{k})$ – upper plots, $G(\mathbf{k}) = G_\parallel(\mathbf{k})$ – lower plots) vs $\ln k$ at $\beta = 1.1$, $h = 0.0003125$, $L = 350$ (empty circles), $\beta = 1.1$, $h = 0.0003125$, $L = 256$ (x); $\beta = 1.1$, $h = 0.000875$, $L = 256$ (squares); $\beta = 1.2$, $h = 0.0004375$, $L = 350$ (solid circles); and $\beta = 1.2$, $h = 0.000875$, $L = 256$ (pluses).
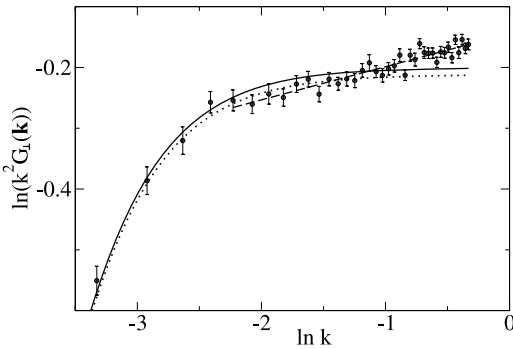
holds asymptotically for small k. According to the standard theory, $\lambda_\perp = 2$ is expected. Our data can be used to test this relation, since, omitting few (5 or 6 at $L = 350$) smallest nonzero k_l values, e.g., at $L = 350$ or $L = 256$, the data for $h = 0.0003125$ and $h = 0.0004375$ with a good enough accuracy correspond to the $h = +0$ limit (at $L = \infty$) in this range of k. While the smallness of the finite-size effects has been already shown in Fig. 4, now we need to test also the influence of finite h to justify this statement. As an example, a set of $\ln G_\perp(\mathbf{k})$ vs $\ln k$ plots for $h = 0.0003125$, 0.0004375 and 0.000875 is shown in Fig. 6 at $\beta = 1.1$ and $L = 256$. Here the size $L = 256$ is chosen for illustration, since more data have been simulated at $L = 256$ than at $L = 350$, whereas the results in both cases are fully consistent with each other. As we can see from Fig. 6, the plots for different fields h tend to merge at large enough k. Besides, the difference between the plot for certain h with those for smaller h values becomes negligible at some $k = k^*(h)$, where $k^*(h)$ increases with h roughly as $\propto h^{1/2}$. We have stated this by analyzing several plots, and it is also quite consistent with (20), since $a(h)$ and $M(h)$ weakly depend on h at $h \to 0$. In particular, the two plots at $h = 0.0003125$ and $h = 0.0004375$ in Fig. 6 well lie on top of each other within the statistical error bars for $k \geqslant k_5$, whereas all three plots do so for $k \geqslant k_7$, where $k_l = 2\pi l/256$ in this case. This behavior at $\beta = 1.1$ is very similar to that at $\beta = 1.2$. Based on such analysis, we have found that our data at the largest sizes are well enough consistent with $G_\perp(\mathbf{k})$ in the thermodynamic limit at $h = +0$ for $k \geqslant k^*(h)$, where $k^*(0.0003125) = k_6$ and $k^*(0.0004375) = k_7$ with $k_l = 2\pi l/L$ at $L = 350$. The necessity to discard some data points at the smallest k values is a disadvantage of the Monte Carlo analysis of this limit. On the other hand, it is particularly interesting to study the behavior of the correlation functions just in this re-
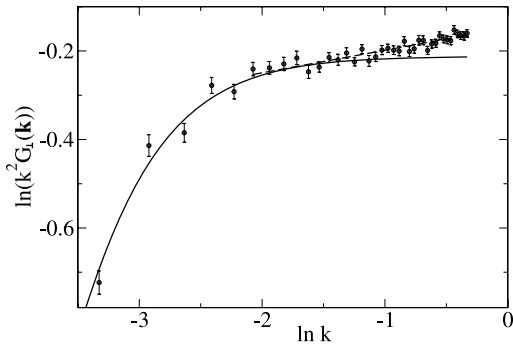
Fig. 6. Logarithm of the transverse correlation function vs $\ln k$ at $\beta = 1.1$ and $L = 256$ for $h = 0.0003125$ (circles), $h = 0.0004375$ (squares) and $h = 0.000875$ (pluses).
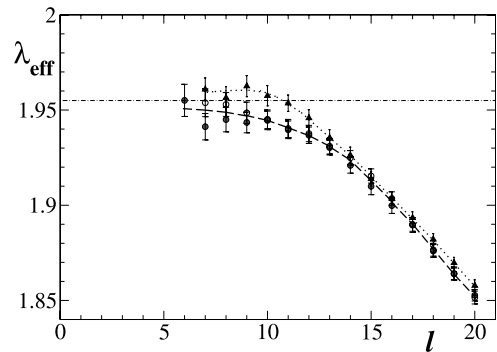

Fig. 7. Logarithm of $k^2 G_\perp(\mathbf{k})$ vs $\ln k$ at $\beta = 1.1$, $h = 0.0003125$ and $L = 350$. Solid and dotted curves correspond to (20) with $a(h) = 1.222$ and $a(h) = 1.236$, respectively, whereas the dashed straight line is the fit to (21) within $k \in [k_6, k_{40}]$.

Fig. 8. Logarithm of $k^2 G_\perp(\mathbf{k})$ vs $\ln k$ at $\beta = 1.1$, $h = 0.0004375$ and $L = 350$. Solid curve corresponds to (20) with $a(h) = 1.236$, whereas the dashed straight line is the fit to (21) within $k \in [k_7, k_{40}]$.

gion, since the Goldstone mode singularity is not shielded by the finite-h effects here.

In Figs. 7, 8 and 9, we have plotted our $\ln(k^2 G_\perp(\mathbf{k}))$ data vs $\ln k$ at $L = 350$ and have compared them with the corresponding theoretical curves calculated from (20). In all three cases considered ($\beta = 1.1$, $10^4 h = 3.125$, 4.375; $\beta = 1.2$, $10^4 h = 4.375$), we observe remarkable systematic deviations from the theoretical curves with $a(h)$ estimated from $k \leqslant k_6$ (solid curves). The overall agreement could be improved, when the values of $a(h)$ are varied slightly (dotted curves). The improvement, however, is insignificant. On the other hand, the data show the existence of a distinct scaling region, where the actual fields practically correspond to the $h = +0$ limit (as discussed before) and the linear fits to (21) (dashed straight lines) are good. Besides, the slopes of these fit lines are not zero, indicating that $\lambda_\perp \neq 2$. More precisely, the fit over $k \in [k_6, k_{40}]$ for $h = 0.0003125$ yields $\lambda_\perp = 1.9454(42)$ (χ^2/d.o.f. $= 1.15$) and

Fig. 9. Logarithm of $k^2 G_\perp(\mathbf{k})$ vs $\ln k$ at $\beta = 1.2$, $h = 0.0004375$ and $L = 350$. Solid and dotted curves correspond to (20) with $a(h) = 1.32$ and $a(h) = 1.335$, respectively, whereas the dashed straight line is the fit to (21) within $k \in [k_7, k_{46}]$.

Fig. 10. The effective exponent λ_{eff} vs l, evaluated by fitting the data to (21) within $k \in [k_l, 4k_l]$, where $k_l = 2\pi l/L$. The data at $L = 350$ and $\beta = 1.1$, $h = 0.0003125$ (solid circles), $\beta = 1.1$, $h = 0.0004375$ (empty circles), as well as $\beta = 1.2$, $h = 0.0004375$ (triangles) have been used for approximation of $G_\perp(\mathbf{k})$ at $h = +0$. The dashed and dotted curves are guides to eye showing the behavior of the effective exponent at $\beta = 1.1$ and $\beta = 1.2$, respectively. The horizontal dot-dashed line indicates the value at which these plots apparently tend to saturate.

the fit over $k \in [k_7, k_{40}]$ for $h = 0.0004375$ gives $\lambda_\perp = 1.9490(42)$ (χ^2/d.o.f. $= 0.90$) at $\beta = 1.1$. The fit over $k \in [k_7, k_{46}]$ for $h = 0.0004375$ yields $\lambda_\perp = 1.9482(32)$ (χ^2/d.o.f. $= 1.42$) at $\beta = 1.2$. Note that the data for different k values are not statistically independent, since they are measured simultaneously. Therefore, the standard errors have been estimated by the jackknife method, considering the results of different simulation bins as statistically independent quantities. Due to the correlations between the fluctuations in $G_\perp(\mathbf{k})$ at different k, the value of χ^2/d.o.f. for a normal (typical) fit over k can be larger than in a case of uncorrelated data, so that all our fits are acceptable. The two fits at $\beta = 1.1$ give well consistent results. Thus, it makes sense to average over them to obtain a more reliable value of $\lambda_\perp$ at this β, i.e., $\lambda_\perp = 1.9472(30)$. It perfectly agrees with $\lambda_\perp = 1.9482(32)$ obtained at $\beta = 1.2$. In such a way, our fits provide a reasonable numerical evidence that the exponent $\lambda_\perp$ is universal and slightly smaller than 2, in agreement with [15,16].

The only disadvantage of our estimation is that the corrections to scaling are not included in (21). The influence of them, however, can be well controlled by looking how the fit results change depending on the range of k. It is shown in Fig. 10. It can be seen that the fit result over the range $[k, 4k]$, denoted as the effective exponent $\lambda_{\text{eff}}(k)$, tends to saturate at certain value near 1.955 (the dot-dashed line in Fig. 10) with decreasing of k. According to the corrections to scaling, proposed by the standard theory, $\lambda_{\text{eff}}(k)$ should be representable by an expansion in integer powers of k, and thus should smoothly (expected linearly) tend to the asymptotic value 2 at $k \to 0$. Thus, the predictions of the standard theory cannot be confirmed by our data. The saturation,

seen in Fig. 10, indicates that the estimated exponent $\lambda_\perp$ is quite insignificantly influenced by the corrections to scaling for small enough values of k used in the linear fits in Figs. 7, 8 and 9. It justifies our estimates of $\lambda_\perp$, considered before, as reasonable. However, one should take into account that the error bars reported for these $\lambda_\perp$ values reflect the statistical errors only and do not include possible systematic errors, i.e., systematic discrepancies between the actually measured effective exponents and the asymptotic ones. In fact, the variations of the effective exponents in Fig. 10 indicate that these discrepancies could be about 0.01. Indeed, according to this behavior, the asymptotic value of $\lambda_\perp$, very likely, is near 1.955 or even 1.96, i.e., by an amount of ~ 0.01 larger than 1.9472(30) or 1.9482(32). For a larger confidence, we state even twice larger than ± 0.01 error bars, thus taking into account both statistical and systematical uncertainties. In such a way, rounding up the latter two values, we obtain an estimate $\lambda_\perp = 1.95 \pm 0.02$. According to the systematic shift to somewhat larger than 1.95 values, observed in Fig. 10, $\lambda_\perp = 1.955 \pm 0.020$ might be a slightly better estimate. Because of absence of rigorous criteria in estimation of systematic errors, the error bars could be stated somewhat different. However, the relatively small variations of the effective exponents for the considered here smallest k values within $k \in [k_6, k_{10}]$ do not give any reason to put them as large as, e.g., ± 0.05. Hence, the data for the transverse correlation function in the actually considered range of the wave vectors, at least, support the idea that $\lambda_\perp < 2$ holds. It agrees with [16], where the relations $d/2 < \lambda_\perp < 2$ and $\rho = (d/\lambda_\perp) - 1$ have been found. The actually estimated exponents $\rho = 0.52 \pm 0.02$ and $\lambda_\perp = 1.955 \pm 0.020$ well satisfy these relations within the error bars.

We have also analyzed the longitudinal correlation function $G_\parallel(\mathbf{k})$. The expected asymptotic behavior in the thermodynamic limit at $h = +0$ is $G_\parallel(\mathbf{k}) \propto k^{-\lambda_\parallel}$ at $k \to 0$. According to the standard theory, $\lambda_\parallel = 4 - d$, i.e., $\lambda_\parallel = 1$ is expected in three dimensions $d = 3$. The prediction of [16] is $\lambda_\parallel = 2\lambda_\perp - d$ with $d/2 < \lambda_\perp < 2$, i.e., $\lambda_\parallel < 1$ at $d = 3$. According to our estimates $\lambda_\perp = 1.95 \pm 0.02$ and $\lambda_\perp = 1.955 \pm 0.020$, it would mean that $\lambda_\parallel = 0.90 \pm 0.04$ or $\lambda_\parallel = 0.91 \pm 0.04$ holds.

The finite-h effects in the actual MC data for $G_\parallel(\mathbf{k})$ are not negligible in the whole range of k values, and we do not observe a distinct scaling region, where the $\ln G_\parallel(\mathbf{k})$ vs $\ln k$ plot is almost linear. However, the behavior of $G_\parallel(\mathbf{k})$ still can be analyzed in terms of effective exponents, which depend on k, h, and slightly also on L. We have considered the effective exponent $\widetilde{\lambda}_{\text{eff}}$. It is defined as an average slope of the $-\ln G_\parallel(\mathbf{k})$ vs $\ln k$ plot within $[k, 2k]$, evaluated from the linear fit of the data within this interval. Here the interval $[k, 2k]$ is chosen so narrow, since the $\ln G_\parallel(\mathbf{k})$ vs $\ln k$ plot is too nonlinear and therefore cannot be well fit by a straight line within a remarkably wider interval as, e.g., $[k, 4k]$ used in the analysis of the transverse correlation function.

The finite-h and finite-size effects are illustrated in Fig. 11. We have determined appropriate region $k > k_0$, where two conditions are satisfied: (1) the discrepancies between the $\ln G_\parallel(\mathbf{k})$ vs $\ln k$ plots for different h values are about 0.1 or smaller, and (2) the finite-size effects are remarkably smaller than the finite-h effects. The corresponding $\ln k_0$ values for $\beta = 1.1$ and $\beta = 1.2$ are indicated by vertical dashed lines in Fig. 11. We have judged about the magnitude of the finite-size effects by comparing the effective exponents at $L = 350$ and $L = 256$ for the smallest h value at the given β. The magnitude of the finite-h effects has been evaluated by comparing the effective exponents at the smallest and largest h values.

The behavior of the effective exponent $\widetilde{\lambda}_{\text{eff}}$ within $k > k_0$ at different values of h and L is shown in Fig. 12 for $\beta = 1.1$ (left) and $\beta = 1.2$ (right). In both cases the plots of the effective exponent decrease below the standard theoretical asymptotic value $\lambda_\parallel = 1$
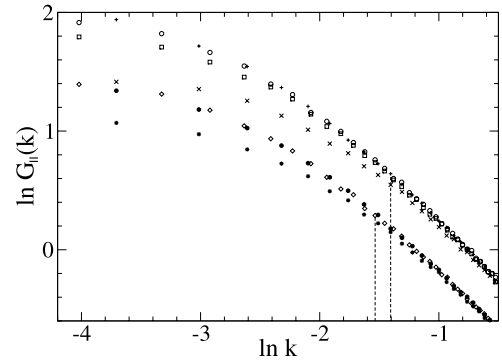

Fig. 11. The $\ln G_\parallel(\mathbf{k})$ vs $\ln k$ plots. The upper curves refer to $\beta = 1.1$ at $L = 350$, $h = 0.0003125$ (empty circles); $L = 256$, $h = 0.0003125$ (pluses); $L = 350$, $h = 0.0004375$ (squares); and $L = 256$, $h = 0.000875$ (x). The lower curves refer to $\beta = 1.2$ at $L = 350$, $h = 0.0004375$ (diamonds); $L = 256$, $h = 0.0004375$ (solid circles); $L = 256$, $h = 0.000875$ (asterisks). The vertical dashed lines indicate the border of the region, where the curves at different fields h agree with certain accuracy (see text) and the finite-size effects are relatively small.

(horizontal dot-dashed line) with decreasing of k. Taking into account the magnitude of the observed here finite-h effects, as well as the smallness of the finite-size effects, it looks very plausible that the true asymptotic exponent has the already mentioned unconventional value about 0.9 (or about 0.91), obtained from our estimates of $\lambda_\perp$ according to the relation $\lambda_\parallel = 2\lambda_\perp - d$. Since the deviations of the $\widetilde{\lambda}_{\text{eff}}$ vs k plots below 1 remarkably exceed the observed finite-h and finite-size effects at $\beta = 1.2$, it does not seem plausible that $\lambda_\parallel = 1$ holds in this case.

5. Conclusions

Monte Carlo simulations of the 4-component vector (or $O(4)$) model in the ordered phase have been performed by a modified Wolff cluster algorithm, measuring magnetization, susceptibility, as well as longitudinal and transverse correlation functions. Based on the simulation results at two couplings $\beta = 1.1$, 1.2 and small external fields $h \geqslant 0.0003125$ for linear system sizes up to $L = 350$, the theoretical predictions for the Goldstone mode singularities have been tested. Our magnetization ($M(h)$) data are in an approximate agreement with the prediction of the standard theory, according to which $M(h) - M(+0) \propto h^\rho$ with $\rho = 1/2$ holds in the thermodynamic limit at $h \to 0$. However, the fits of the magnetization, as well as the longitudinal susceptibility data suggest that the exponent ρ, probably, has a larger value – about 0.52 (Section 3). In particular, an estimate $\rho = 0.52 \pm 0.02$ has been obtained from the magnetization data, taking into account both statistical and systematical uncertainties. Apart from the exponent ρ, more accurate than previously reported in literature values of the spontaneous magnetization $M(+0)$ have been obtained (Section 3).

As a test of validity, we have verified that the simulated transverse correlation function at the largest lattice sizes and smallest fields is consistent with the exact relation (19). For small values of h, our data show a distinct scaling region, where the transverse correlation function behaves as $\propto k^{-\lambda_\perp}$ with $\lambda_\perp = 1.9472(30)$ evaluated at $\beta = 1.1$ and $\lambda_\perp = 1.9482(32)$ evaluated at $\beta = 1.2$. In fact, these are the effective exponents in the fitted wave–vector range $k \in [k_6, k_{40}]$ and $k \in [k_7, k_{40}]$, respectively, where $k_l = 2\pi l/350$. Only the statistical error bars of one standard deviation are indicated here. The possible systematic errors, defined as systematic discrepancies between the actually measured and asymptotic values of $\lambda_\perp$, have been evaluated by analyzing the variations of the effective exponents (see Fig. 10), leading to
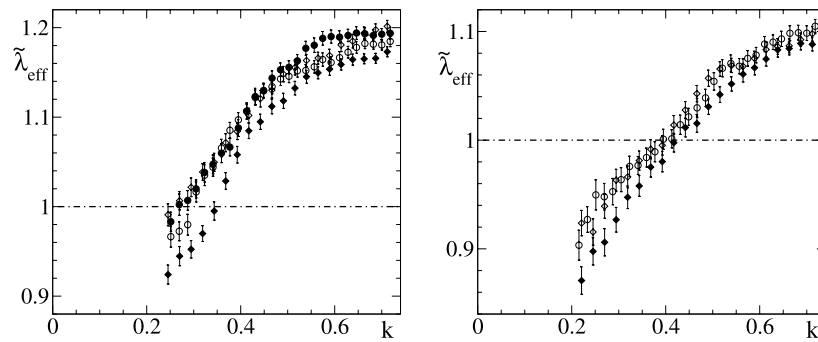
Fig. 12. The effective exponent $\widetilde{\lambda}_{\text{eff}}$ vs k at $\beta = 1.1$ (left) and $\beta = 1.2$ (right) for $L = 350$, $h = 0.0003125$ (solid circles); $L = 350$, $h = 0.0004375$ (empty circles); and $L = 256$, $h = 0.000875$ (solid diamonds). The empty diamonds correspond to $L = 256$ at the smallest h (0.0003125 for $\beta = 1.1$ and 0.0004375 for $\beta = 1.2$). The horizontal dot-dashed line indicates the standard asymptotic value $\lambda_{\parallel} = 1$.

the estimates $\lambda_{\perp} = 1.95 \pm 0.02$ and $\lambda_{\perp} = 1.955 \pm 0.020$ (Section 4). These results suggest that the exponent $\lambda_{\perp}$ is universal, but slightly smaller than 2, in disagreement with the standard theoretical prediction $\lambda_{\perp} = 2$ and in agreement with [15,16]. The analysis of the longitudinal correlation function provides an extra evidence of unconventional behavior. According to the variations of effective exponents (see Fig. 12) it looks very plausible that $\lambda_{\parallel} = 2\lambda_{\perp} - d \approx 0.9$ holds for the exponent $\lambda_{\parallel}$ (defined by $G_{\parallel}(\mathbf{k}) \propto k^{-\lambda_{\parallel}}$ at $k \to 0$) in agreement with this relation between the exponents found in [16] and our estimates of $\lambda_{\perp}$, and in disagreement with the standard theoretical prediction $\lambda_{\parallel} = 1$ at $d = 3$.

Acknowledgements

References

[1] I.D. Lawrie, J. Phys. A 18 (1985) 1141.
[2] P. Hasenfratz, H. Leutwyler, Nucl. Phys. B 343 (1990) 241.
[3] U.C. Tuber, F. Schwabl, Phys. Rev. B 46 (1992) 3337.
[4] L. Schäfer, H. Horner, Z. Phys. B 29 (1978) 251.
[5] R. Anishetty, R. Basu, N.D. Hari Dass, H.S. Sharatchandra, Int. J. Mod. Phys. A 14 (1999) 3467.
[6] I. Dimitrović, P. Hasenfratz, J. Nager, F. Niedermayer, Nucl. Phys. B 350 (1991) 893.
[7] J. Engels, T. Mendes, Nucl. Phys. B 572 (2000) 289.
[8] J. Engels, S. Holtman, T. Mendes, T. Schulze, Phys. Lett. B 492 (2000) 492.
[9] J. Kaupužs, R.V.N. Melnik, J. Rimshans, Eur. Phys. J. B 55 (2007) 363.
[10] J. Kaupužs, R.V.N. Melnik, J. Rimšāns, Commun. Comput. Phys. 4 (2008) 124.
[11] A. Pelissetto, E. Vicari, Phys. Rep. 368 (2002) 549.
[12] U. Wolff, Phys. Rev. Lett. 62 (1989) 361.
[13] Ma Shang-Keng, Modern Theory of Critical Phenomena, W.A. Benjamin, Inc., New York, 1976.
[14] W.H. Press, B.P. Flannery, S.A. Teukolsky, W.T. Vetterling, Numerical Recipes – The Art of Scientific Computing, Cambridge University Press, Cambridge, 1989.
[15] J. Kaupužs, Latvian J. Phys. Tech. Sci. 5 (2002) 31–36.
[16] J. Kaupužs, e-print cond-mat/0202416v4, 2004.
[17] J. Kaupužs, Ann. Phys. (Leipzig) 10 (2001) 299.